Donné-Op den Kelder, G. M., Hille, J. D. R., Dijkman, R., de Haas, G. H., & Egmond, M. R. (1981) *Biochemistry 20*, 4074-4078.
Donné-Op den Kelder, G. M., de Haas, G. H., & Egmond, M. R. (1983) *Biochemistry 22*, 2470-2478.
Egmond, M. R., Slotboom, A. J., de Haas, G. H., Dijkstra, K., & Kaptein, R. (1980) *Biochim. Biophys. Acta 623*, 461-466.
Egmond, M. R., Hore, P. J., & Kaptein, R. (1983) *Biochim. Biophys. Acta 744*, 23-27.
Ghosh, S., Weers, J. G., Petrin, M. & Maki, A. H. (1984) *Chem. Phys. Lett. 108*, 87-93.
Gupta, C. M., & Bali, A. (1981) *Biochim. Biophys. Acta 663*, 506-515.
Hendrickson, H. S., Trygstad, W. M., Loftness, T. L., & Sailer, S. L. (1981) *Arch. Biochem. Biophys. 212*, 508-514.
Hershberger, M. V., Maki, A. H., & Galley, W. C. (1980) *Biochemistry 19*, 2204-2209.
Hille, J. D. R. (1983) Ph.D. Thesis, State University of Utrecht, Utrecht, The Netherlands.
Hille, J. D. R., Egmond, M. R., Dijkman, R., van Oort, M. G., Jirgensons, B., & de Haas, G. H. (1983a) *Biochemistry 22*, 5347-5353.
Hille, J. D. R., Egmond, M. R., Dijkman, R., van Oort, M. G., Sauve, P., & de Haas, G. H. (1983b) *Biochemistry 22*, 5353-5358.
Maki, A. H. (1984) in *Biological Magnetic Resonance* (Berliner, L. J., & Reuben, J., Eds.) pp 187-294, Plenum Press, New York.
Maki, A. H., & Co, T. (1976) *Biochemistry 15*, 1229-1235.
Mao, S. Y., Maki, A. H., & de Haas, G. H. (1985) *FEBS Lett. 185*, 71-75.
Nieuwenhuizen, W., Kunze, H., & de Haas, G. H. (1974) *Methods Enzymol. 32B*, 147-154.
Pieterson, W. A., Volwerk, J. J., & de Haas, G. H. (1974) *Biochemistry 13*, 1439-1445.
Slotboom, A. J., Jansen, E. H. J. M., Vlijm, H., Pattus, F., Soares de Araujo, P., & de Haas, G. H. (1978) *Biochemistry 17*, 4593-4600.
Slotboom, A. J., Verheij, H. M., & de Haas, G. H. (1982) in *Phospholipids* (Hawthorne, J. N., & Ansell, G. B., Eds.) pp 359-434, Elsevier Biomedical Press, Amsterdam, New York, and Oxford.
Soares de Araujo, P., Rosseneu, M. Y., Kremer, J. M. H., van Zoelen, E. J. J., & de Haas, G. H. (1979) *Biochemistry 18*, 580-586.
van Dam-Mieras, M. C. E., Slotboom, A. J., Pieterson, W. A., & de Haas, G. H. (1975) *Biochemistry 14*, 5387-5394.
van Egmond, J., Kohler, B. E., & Chan, I. Y. (1975) *Chem. Phys. Lett. 34*, 423-426.
Verheij, H. M., Slotboom, A. J., & de Haas, G. H. (1981) in *Reviews of Physiology, Biochemistry and Pharmacology* (Vogt, W., Ed.) pp 91-203, Springer-Verlag, Heidelberg.
Volwerk, J. J., & de Haas, G. H. (1982) in *Lipid-Protein Interactions* (Jost, P.C., & Griffith, O. H., Eds.) Vol. 1, p 69-149, Wiley, New York.
Volwerk, J. J., Jost, P. C., de Haas, G. H., & Griffith, O. H. (1984) *Chem. Phys. Lipids 36*, 101-110.

Protoheme–Carbon Monoxide Geminate Kinetics†

Michael C. Marden,* E. Starr Hazard III, and Q. H. Gibson
Department of Biochemistry, Cellular and Molecular Biology, Cornell University, Ithaca, New York 14853
Received November 14, 1985; Revised Manuscript Received January 21, 1986

ABSTRACT: Recombination kinetics of CO to protoheme after laser photolysis have been measured vs. temperature and viscosity. A 25-ns laser pulse was focused on the sample to produce an excitation rate of 10^9/s per heme. This temporarily populates the heme–CO state of dissociated pairs which either separate or recombine on a picosecond time scale in viscous glycerol–water solutions. From the equilibrium amplitude of the fraction dissociated during the laser pulse, the geminate recombination rate constant is calculated to be 3×10^9/s. This rate coefficient is only weakly dependent on temperature or viscosity. As previously observed the fraction that escapes depends on the solvent viscosity [Marden, M. C. (1983) Ph.D. Thesis, University of Illinois–Urbana]. A model consisting of a single barrier plus diffusive escape is used to simulate the kinetics during and just after the flash.

The kinetics of carbon monoxide binding to protoheme has been extensively studied on a microsecond time scale. After photodissociation of CO from protoheme, a single bimolecular process has been observed and characterized as a function of temperature and viscosity (Alberding et al., 1976; Hasinoff, 1977; Marden, 1980). The observed amplitude of this process decreases as the solvent viscosity increases. This implies either that the photosensitivity decreases or that a fast geminate process exists which accounts for the missing fraction of the change in absorbance. A geminate phase has been seen for protoheme in frozen solvents when there is no escape of the ligand; values for the rate in the liquid phase have been extrapolated from below 100 K as 10^9/s (Alberding et al., 1976) and 26×10^9/s (Doster et al., 1982). Geminate kinetics have been observed in heme proteins on a nanosecond/microsecond scale (Austin et al., 1975; Duddell et al., 1980; Lindqvist et al., 1981) and later extended to the picosecond time scale (Chernoff et al., 1980; Friedman et al., 1985).

Model compounds have been prepared that can approximate the oxygen binding equilibrium curves observed in proteins. This implies that the ratio of the on/off rates is correct; a more

† This work was supported in part by National Institutes of Health Grant GM-14276 and National Science Foundation Grant 79-10446.

0006-2960/86/0425-2786$01.50/0

critical test of model compounds is in the actual kinetics. In stopped-flow experiments, the reactants are initially uniformly distributed and the bimolecular reaction rate is measured. In flash photolysis, the reactants are initially in pairs, and information is obtained on the immediate reactivity (geminate phase), the escape from the reaction site, and the final bimolecular process. In this study all these steps of the kinetics are considered to determine whether protoheme serves as a useful model for proteins.

Measurements of the geminate phase of protoheme–CO are necessary in order to study the effects of the globin on the protein kinetics. When protoheme combines with globin forming a hemoprotein, the physical properties of both are substantially changed. Absorption spectra are shifted, protein fluorescence is quenched, and the complete protein is stable to higher temperatures and pressures. The most significant change biologically is that, in the protein, oxygen can reversibly bind to the iron atom of the heme group in the protein.

To observe the geminate phase, it is necessary that not all ligands escape to the solvent; water is not a good solvent, since nearly all ligands escape and rebind via the bimolecular process. High viscosity solvents can be used to control the fraction rebinding via the geminate phase.

The duration of the geminate phase can be estimated from the diffusive escape rates. Since a ligand like CO migrates approximately 20 Å in 1 ns in water, the ligand and heme will be correlated only on the picosecond time scale. The experiment therefore requires a rapid detection system to record the changes during and just after the laser pulse.

Materials and Methods

A cavity dumped dye laser (Phase-R, 2100B) was used for photodissociation. Pulses of 25 ns were obtained with an energy of 75 mJ with Rhodamine (575 nm) (Exciton) or 25 mJ with coumarin (545 nm) (Phase-R). A steady-state technique was used to determine the geminate recombination rate. The laser pulse was focused on the sample to obtain a rate of 10^9 photons/s per heme as determined by dissociation of MbCO or heme–CO at low viscosity with pulses of reduced energy. A photostationary ratio of liganded and dissociated states is established with the laser intensity determining the off rate and the geminate recombination the on rate.

A Xe arc lamp was focused within the laser spot and pulsed to obtain better signal to noise during the first 100 μs. The transmitted light passed through a monochromator and was measured with a RCA 1P28 photomultiplier. The signal was recorded on an HP 1727A oscilloscope using the 50-Ω load, resulting in an overall response time of less than 3 ns. Photographs were taken of the oscilloscope screen, expanded, and digitized to obtain plots of absorption vs. time.

Glycerol–water mixtures were used to obtain samples at high viscosity. A range of greater than 10^5 in viscosity was covered, from water to cooled glycerol (viscosity units are poise = P = 0.1 kg m/s). The glycerol percentage was determined from the infrared spectrum measured on a Cary 14 in the region 1300–2000 nm. Pure glycerol shows a low absorbance at 1940 nm (0.1 OD/mm); each percent water increased the absorbance by an additonal 0.08 OD in a 1-mm cell.

Typical samples were 60μM heme in 100 mM borate buffer, pH 9. Sodium dithionite was used for reduction of the heme in the presence of CO or KCN.

Protoheme (Sigma) was dissolved in 0.1 M NaOH before transfer to the final solvent conditions. Dimethyldeuterohemedisulfonate (DDD-heme) was the gift of Dr. R. L. J. Lyster. The samples were in 1-mm cuvettes in contact with an aluminum block. Temperature was controlled by varying the current through a thermoelectric chip (Melcor).

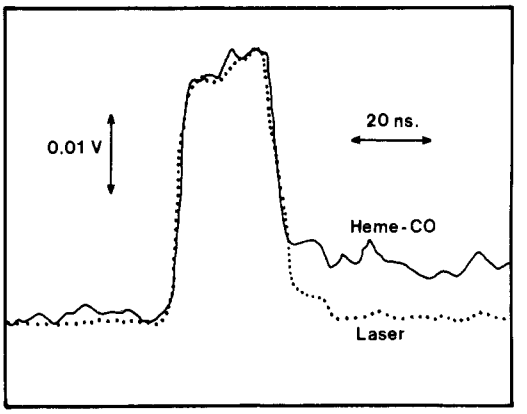

FIGURE 1: Laser pulse (···) and 430-nm light transmission through a sample of protoheme–CO in 96% glycerol at −36 °C. During the laser pulse each heme absorbs a photon on the average once per nanosecond.

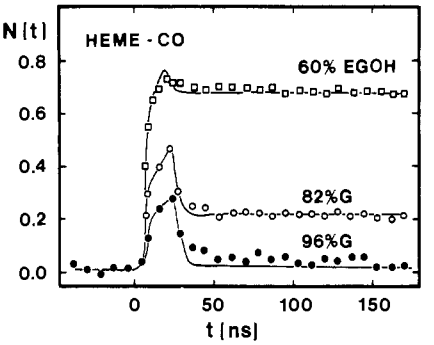

FIGURE 2: Fraction dissociated vs. time for protoheme–CO in 60% ethylene glycol at −38 °C, 82% glycerol at −30 °C, and 96% glycerol at −30 °C. Solid lines are simulations for diffusive escape from a single barrier.

Results

Kinetic measurements were made on four systems: heme–CO, CN–heme–CN, CN–heme–CO, and DDD-heme–CO. Sample kinetics of the dissociation and subsequent rebinding of CO to protoheme are shown in Figure 1. The profile of the laser pulse is also shown, nearly a rectangular shape of width 25 ns. Each heme absorbs a photon on the average every 1 ns. If the rebinding time constant is comparable to or slower than several picoseconds, the deoxy state will be observably populated. At the end of the laser pulse, the ligands will either rebind with the geminate rate or migrate away from the binding site.

The data shown in Figure 1 are at high viscosity, 96% glycerol w/w at 230 K where the viscosity is 1000 P; in this case few ligands escape to the solvent. Since the rebinding and laser photodissociation times are both short compared to the pulse length, the absorbance change closely follows the laser pulse. The change is only one-fourth the maximum signal observed at low viscosity, implying that the geminate rebinding rate is 3 times greater than the dissociation rate.

The results in different solvents are shown in Figure 2. In a low viscosity solvent like ethylene glycol or water, a high fraction of the ligands escape and rebind via the slower bimolecular process. As the percentage of glycerol is increased, the higher viscosity slows the diffusive escape and the geminate phase dominates.

The results at different temperatures for DDD-heme–CO in 95% glycerol are shown in Figure 3. The dominant change is due to solvent viscosity rather than temperature. At high

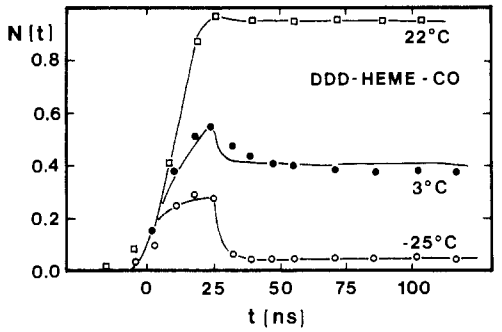

FIGURE 3: Fraction dissociated vs. time for DDD-heme–CO in 95% glycerol at 22, 3, and −25 °C. Solid lines as in Figure 2.

temperature (low viscosity), the ligand preferentially escapes and later rebinds via the bimolecular phase. The solid lines in Figures 2 and 3 are simulations using a model with a single barrier and a diffusive escape in three dimensions. In three dimensions the number of solvent sites available to the ligand increases as the cube of the distance migrated. The diffusive escape rate depends on the ligand diffusivity which in turn is highly correlated with the bulk solvent viscosity (Jordan et al., 1956).

The model assumes three general states: A, ligand bound; B, dissociated pairs with the ligand at the barrier; S, any site in the solvent. Absorption of a photon causes a change in the absorption spectrum from ligand bound (state A) to unbound (state B) within a few picoseconds (Reynolds et al., 1981; Martin et al., 1983). From state B there is competition between geminate rebinding with rate k_{BA} and diffusive escape modeled as jumps within the solvent. It has previously been shown that the rate and amplitude of the bimolecular process for heme–CO show a viscosity dependence (Beece et al., 1980; Marden, 1980).

A necessary condition of the diffusion model is that the escape rate scale with ligand diffusivity. However, the escape rate is not a directly observable quantity, and tables are not available for CO diffusivity in glycerol–water mixtures. We therefore relate a derived function of this rate to the solvent viscosity. In a model of competition between rebinding with rate k_{BA} and an overall escape rate of k_{BS}, the fraction escaping after dissociation is $N^{out} = k_{BS}/(k_{BS} + k_{BA})$. k_{BA} was found to have a weak dependence on viscosity and temperature (<1 kJ/mol). From the reciprocal relation

$$1/N^{out} = 1 + k_{BA}/k_{BS} \quad (1)$$

it can be seen that either k_{BS} or the observable N^{out} can be tested for a correlation with ligand diffusivity. Measurements were made of N^{out} vs. temperature and viscosity with a low laser energy to avoid multiple dissociation.

In a given solvent, $1/k_{BS}$ scales with viscosity within 20% for the systems studied. This scaling is shown for CN–heme–CN and heme–CO in 79% glycerol in Figure 4, without any correction for k_{BA}. The scaling between different solvents of more than 60% glycerol was also good, but inclusion of 0–60% glycerol showed deviations of more than a factor of 3, probably due to deviations in correlation between diffusivity and viscosity (Jordan et al., 1956).

Data for CN–heme–CO and heme–CO were similar, indicating that CO is dissociated in both cases. Data for DDD-heme–CO were also similar to those of heme–CO, except that k_{BA} was 2 times lower. As expected from the diffusion model, more ligands escape when the binding rate is smaller.

Data for CN–heme–CN appear anomalous. The fraction escaping was only 3 times less than that of heme–CO, yet no

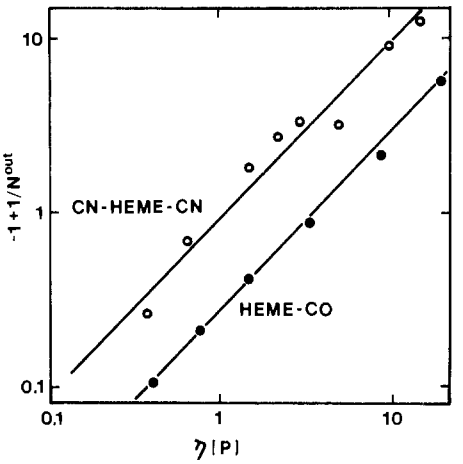

FIGURE 4: Test of correlation of diffusive escape rate k_{BS} with viscosity, as indicated by a straight line for $(-1 + 1/N^{out}) = k_{BA}/k_{BS}$ vs. viscosity.

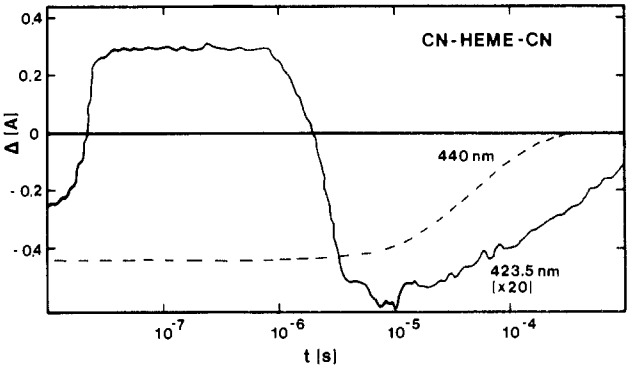

FIGURE 5: Recombination kinetics of CN–heme–CN measured at 440 nm with less than one photon per heme (---). Solid line is the kinetics at high photolysis energies with the observation at the isobestic point (423.5 nm) for the reaction observed with low energy ($\Delta A \times 20$).

geminate phase was observed. Additional measurements were made to detect dissociation of both CN molecules from CN–heme–CN. At laser energies providing less than one photon per heme, the signal for dissociation of the first CN could be observed alone. The difference spectrum had peaks at 440 and 415 nm, with an isobestic point at 423.5 nm. The photolysis energy was then increased, and observation at 423.5 nm revealed additional processes, implying formation of new spectral forms distinct from CN–heme–CN and its photoproduct at low laser energy. Results in Figure 5 show the kinetics for CN–heme–CN in 100 mM sodium borate, pH 9.2. The dashed line is the kinetic trace at low laser energy, with observation at 440 nm, showing the bimolecular rebinding of CN. The solid line is the trace observed at the isobestic point (423.5 nm) with high laser energy. The first process is pH dependent; the two slower processes depend on both pH and CN concentration.

Simulations. Kinetics are generated with a sequential model consisting of a single barrier plus a random walk:

$$A \rightleftharpoons B \rightleftharpoons S_2 \rightleftharpoons S_3 \rightleftharpoons S_4 \ldots \quad (2)$$

The rate k_{BA} for binding depends on the protein ligand system. Rate k_{AB} is proportional to the photolyzing light intensity. All other rates are equal to the random walk jump frequency k_J.

A one-dimensional diffusion model can be solved exactly (Appendix) or treated as a multiple barrier problem and is characterized by a slope $^1/_2$ on a log–log plot of the fraction unbound $N(t)$ vs. time. An alternative method is to approximate the decreasing ligand population in well B (Marden, 1982), but it is not an exact solution of the diffusion equation.

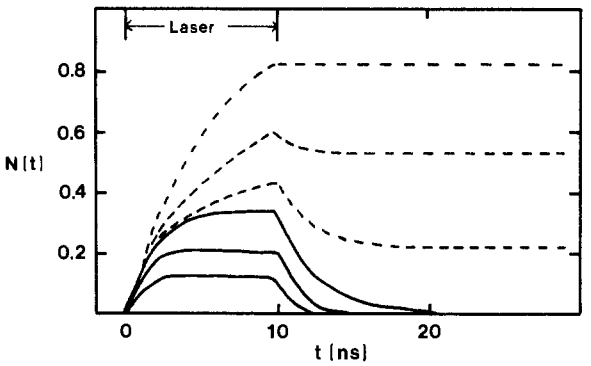

FIGURE 6: Simulations for the model of a single barrier plus a random walk in three dimensions. The three lower curves are with zero difussion with $k_{AB} = 2 \times 10^8$ s^{-1} and $k_{BA}/10^8 = 4$, 8, and 16 s^{-1}. The upper curves show increasing rates for the diffusive steps $k_J/10^8 = 4$, 0.4, and 0.1 s^{-1} (top to bottom).

In three dimensions, no closed form solutions exist, and simulations were made by numerical integration. The three-dimensional (3D) case was still treated as a sequential model, but now a sequence of spherical shells in which the number of sites increases as the cube of the shell number. Well B is treated as the first shell with a single site. For each time slice the population of each shell is adjusted in the program as $P(i) = P(i) + \Delta P(i)$ with

$$\Delta P(i) = k_J \Delta t[P(i-1)i^d + P(i+1)i^d - P(i)[(i-1)^d + (i+1)^d]] \quad (3)$$

as required by the equilibrium condition that all sites are uniformly populated $P(i) = P(i+1)[i/(i+1)]^d$. d is the dimension of the problem; the factors with d are not needed for the one-dimensional case. As in any computer problem, a finite number of sites is used; nine shells were sufficient for most simulations in three dimensions.

Sample simulations are shown in Figure 6. The three lower curves are with negligible k_J so the ligand is trapped in well B. The curves rise with rate $k_{AB} + k_{BA}$ to a steady-state value:

$$N(\text{steady state}) = k_{AB}/(k_{AB} + k_{BA}) \quad (4)$$

Since k_{AB} is known from the laser intensity, the geminate rebinding rate k_{BA} can be calculated from the steady-state amplitude. Simulations in Figure 6 show how the amplitude varies with $k_{BA}/10^8 = 4$, 8, and 16 s^{-1} and $k_{AB} = 2 \times 10^8$ s^{-1}. As the diffusive escape becomes comparable in rate to the rebinding, ligands escape during the laser pulse, seen as the secondary rise in $N(t)$. Thus, an observable signal is obtained when k_J competes with k_{BA}. A picosecond study would provide a direct measurement of k_{BA}, but only the overall escape rate k_{BS} could be deduced from the fraction escaping. In general the parameters k_{BA} and k_J were varied to obtain fits to the data with an average error of less than 10%.

In 3D the population of well B drops significantly after several diffusive jumps as many new sites become available to the ligand resulting in a finite escape probability. In an infinite one-dimensional channel, on the other hand, no ligand will escape and the kinetics show a slope $^1/_2$ on a plot of log (N) vs. log (t). Since the kinetics of many proteins show the slope $^1/_2$ characteristic of the one-dimensional model, simulations are presented in Figure 7. This model is applied to the kinetics of MbO_2, shown in Figure 8, using a channel of finite length. When the ligands reach the solvent, they can diffuse in 3 dimensions. They also have a larger diffusivity outside the protein, implied by their long correlation time. One additional parameter is required for the bimolecular phase with rate $P_B k_{BA} N^{out}$, a form derived by Noyes (1961), where P_B is the equilibrium probability that the ligand is in well B. Thus, geminate and bimolecular phases are treated as binding over the same barrier, simply with very different populations of well B. The geminate phase is not exponential due to the time-dependent decay of $P_B(t)$.

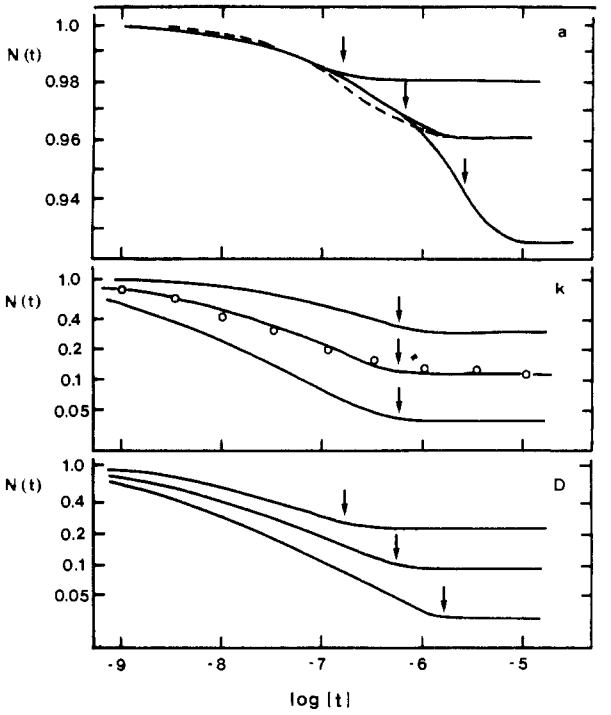

FIGURE 7: Simulations using the one-dimensional diffusion model. Plots are log $N(t)$, the fraction unbound, vs. log t (in seconds). The top section shows variation of the channel length $a = 0.5$, 1, and 2 nm (top to bottom) with $k = 0.038$ cm/s and $D = 9.6 \times 10^{-9}$ cm^2/s. The dashed line is a single-exponential fit to data of MbCO in water at 25 °C (Henry et al., 1983). The middle section "k" is for $k_{BA} = 0.2$, 0.65, and 2 cm/s (top to bottom) with $a = 1$ nm and $D = 8 \times 10^{-9}$ cm^2/s. Data (O) shown are for the β chain of Hb-Zurich–CO in 79% glycerol at 300 K (Dlott et al., 1983). The lower section, "D", is with $D = 3.16 \times 10^{-8}$, 1×10^{-8}, and 0.316×10^{-8} cm^2/s with $a = 1$ nm and $k = 1$ cm/s. The arrows mark the escape time.

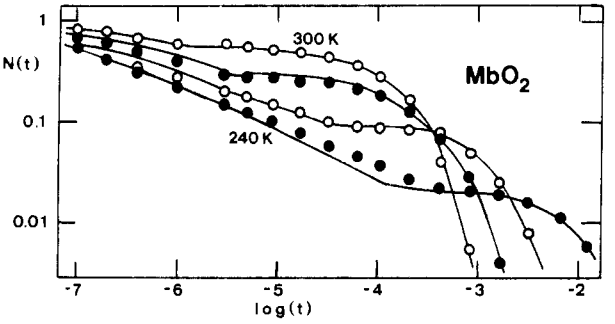

FIGURE 8: Kinetics of oxygen recombination to Mb in 79% glycerol at 240, 260, 280, and 300 K (Beece, 1983). Solid lines are simulations using the one-dimensional diffusion model.

Discussion

The results demonstrate that protoheme–CO has a geminate phase, as previously observed with heme proteins. The geminate rate is 100–500 times faster than those observed for HbCO and MbCO, respectively, but only 6 times faster than the β chain of Hb-Zurich (Dlott et al., 1983). Thus, the protein appears to decrease the rate of crossing the ligand–iron barrier.

In protoheme, a simple escape to the solvent in three dimensions fits the data vs. temperature and viscosity. The ligand is correlated with the heme for only a few nanoseconds

even at high viscosity. The correlation time (duration of the geminate phase) shows another major difference between heme and the heme proteins. Many heme proteins in viscous solvents show a geminate phase which continues over many decades in time with a slope $^1/_2$ on a log–log plot, as observed in one-dimensional simulations. The kinetics depend on the geometry of the ligand channel and whether the protein can be treated as a uniform medium.

The time scale of the geminate phase implies that the diffusivity inside the protein escape channel must be much less than that of the bulk solvent (Marden, 1982). If not, the ligand should have become uncorrelated with its original heme much sooner, as observed for protoheme.

The one-dimensional diffusion model (Appendix) closely approximates the special case of the multiple barrier model when all the outer rates are set equal. This results in a model with fewer parameters but loss of flexibility in fitting kinetics showing discrete processes of differing rates. Rather than approximating the data as a sum of many independent exponentials, the diffusion model leads to a fixed nonexponential shape. The diffusion model is therefore easier to disprove, if there are exponential processes well separated temporally. Cases such as MbO_2 (Figure 8) and Hb-Zurich (Figure 7) do not show gaps between processes and suggest a more uniform diffusion processes.

Another difference is that the multiple barrier model collapses to a single exponential in the high viscosity limit when the ligand is trapped in well B. In the solution of the diffusion equation (Appendix) the nonexponential shape of the geminate phase is invariant. In most heme protein–ligand data, the kinetics still show the nonexponential behavior. This problem was overcome in the multiple barrier model by using a distribution of rates for k_{BA}, as evidenced from low-temperature studies, and a relaxation time to preserve the exponential shape of the final bimolecular process (Austin et al., 1975).

The diffusion model also suggests that the migration behavior should be similar for ligands of similar size. The kinetics may appear different since k_{BA} depends on the ligand, but the escape times (marking the end of the geminate phase) should be similar. Despite a variation of nearly a factor of 100 in the escape times comparing leghemoglobin to Mb (Stetzkowski et al., 1985), oxygen remains a factor of 2–3 times faster than CO. Oxygen also has a higher diffusivity through membranes and some types of rubber.

The simulations shown in Figures 2 and 3 start with all the ligands in the bound state A and therefore include the dissociation phase. The steady state between the geminate rebinding rate k_{BA} and the dissociation rate k_{AB} (proportional to the laser power) is attained within the first 10% of the laser pulse width. In a high viscosity solvent, few ligands escape, and the steady-state deoxy population follows the rectangular shape of the laser pulse. When the viscosity is sufficiently low that the escape rate competes with the binding rate, ligands escape to the solvent during the pulse. This effect is seen in the data and simulation as the ramp up in $N(t)$ during the pulse. At the end of the pulse, the population of well B decays rapidly and $N(t)$ decreases to the amplitude of the bimolecular phase.

The simulation uses a rate for jumping between sites in the solvent k_J which must agree with the known values of the ligand diffusivity in the solvent as $D = k_J d_J^2/6$, with d_J the average distance jumped (Noyes, 1956). Alternatively one can compare the overall escape rate $k_{BS} \cong k_J/6$, which only requires values of k_{BA} and N^{out}. For example, $N^{out} = {}^1/_2$ in 79% glycerol w/w at −5 °C, where the viscosity $\eta = 400$ cP. Assuming Stokes' law, $D \propto 1/\eta$, then the present simulations agree with the estimated diffusivities for $d_J = 0.4$ Å. The value of D for oxygen in 80% glycerol is 10 times larger than predicted by Stokes law (Jordan et al., 1956). If the same is true for CO, then $d_J \cong 1$ Å which is a reasonable value for atomic displacements.

Quantum Yield. One basic question in flash photolysis of heme proteins is the quantum yield. Is the yield at sufficiently short observation times always 1, or do some systems absorb photons without any ligand dissociation? The data for heme–CO agree with the assumption that the yield at short times is 1. Previous data showing a decreased amplitude were collected with too slow a system to observe the fast geminate phase.

CN–heme–CN, however, which does not show a geminate phase, seems to represent a counter example to the simple sequential model used for heme–CO and other systems. It could be suggested that the geminate phase is much faster and beyond detection with the present equipment. This would then imply that few ligands should escape, since the fraction that escapes is a result of competition between the geminate barrier rate and the rate for migration away from the iron atom. The heme–CN data show an escape probability only 3 times less than that of heme–CO. The paradox is that heme–CN shows a decreasing amplitude of the bimolecular process at high viscosity, as observed with heme–CO, without evidence of the competing geminate phase.

The basic assumption for most heme–ligand systems is a quantum yield of 1 for dissociation to a state B with deoxy spectrum from which the ligand may rebind or escape. The CN paradox may be resolved formally by supposing that the spectra of species A and B are similar, possibly due to an electrostatic interaction. The geminate binding from B to A would then not be detected by spectral observation; however, this would imply a slower rate for the formation of the deoxy species. The CN paradox remains an open question, and the only conclusion at this time is that well B for CN is not the same as for CO.

The results with CN–heme–CN at high photolysis energies (Figure 5) indicate that the second CN can be photodissociated, but with a low yield. The subsequent reactions would then be a competition of OH and CN binding, with the final slow process a replacement of OH by CN. This type of experiment is useful in determining the reaction rates of OH with heme; however, a full spectral analysis of these weak signals would be required to permit the chemical forms and their kinetics to be assigned.

Another comparison of heme with the proteins is in the bimolecular rate. Despite a factor of 500 increase in geminate rate comparing heme–CO to MbCO, the bimolecular rate k_{on} is only 30 times faster. This implies that the equilibrium concentration in well B is over 10 times higher for the protein, suggesting a higher volume or solubility. Assuming a solvent ligand concentration c (M) for the case of heme–CO, a volume of well B can be calculated as $V_B = (k_{on}/k_{BA})(1600c) \cong 100$ Å^3, which is the volume of a hemisphere between radii of 2 and 4 Å.

Conclusions. Protoheme–CO shows a geminate recombination phase which may be an upper limit for the protein systems. The duration of the geminate phase at high viscosity is more than a factor of 10^5 longer for MbCO than for heme–CO. This implies a large hindrance of escape by the protein to obtain such large correlation times. The geminate rate coefficients differ by a factor of 500. This rate is important because it represents the rate-limiting step in the ligand

association in solvents of low viscosity. The simulated escape rates are in agreement with observed diffusivities for diffusive jumps of atomic size.

CN–heme–CN represents a case where the escape properties are similar to heme–CO, yet the geminate phase is absent. Data at high laser power indicate that the second CN may be dissociated with low yield.

Acknowledgments

We thank C. Kimble for technical assistance and Dr. R. L. J. Lyster of the National Institute for Research in Dairying in Reading, England, for his gift of DDD-heme.

Appendix

One-Dimensional Diffusion Model. Solutions for the one-dimensional diffusion equation

$$\partial P/\partial t = D\partial^2 P/\partial x^2 \quad \text{(A1)}$$

have been catalogued by Carslaw and Jaeger (1959). The problem of interest for flash photolysis is when the reactants are initially in pairs. This is the initial condition of a point source, whose Green's function solutions have been solved for a variety of boundary conditions. The reaction at $x = 0$ is modeled by the radiation boundary condition:

$$\partial P/\partial X = RP = (k/D)P \quad \text{(A2)}$$

with k a second-order reaction rate (Collins & Kimball, 1949). The migration through the channel occurs to a length $x = a$; this end is in contact with the solvent at a fixed level $P(a,t) = c \ll 1$. The solution with $c = 0$ and the ligands initially localized at $x = 0$ is given as an infinite sum (Carslaw & Jaeger, 1959, p 358). The kinetics are calculated from the flux at $x = 0$ as

$$N(t) = 1 - \int_0^t k_{BA} P(0, t')\, dt' \quad \text{(A3)}$$

After integration, the formula is

$$N(t) = 1 + 2S\sum_{n=1}^{\infty}(A_n^2 + S^2 + S)^{-1}(-1 + \exp(-DA_n^2 t/a^2) \quad \text{(A4)}$$

with $S = Ra$ and the A_n values are solutions of $\tan(A) = -A/S$. The escape probability is calculated from the long time limit:

$$N^{out} = 1 - 2S\sum_n (A_n^2 + S^2 + S)^{-1} = 1/(1 + S) \quad \text{(A5)}$$

This model has a specific form for the kinetics. With large channel length a, $N(t)$ is approximately $\exp[-k(t/D)^{1/2}]$ at short times and $0.56/[k(t/D)^{1/2}]$ at long times. The shape of the geminate phase on a log–log plot is invariant, which facilitates data simulation. Sample simulations are shown in Figure 7.

The top section marked "a" of Figure 7 shows that as the channel length increases (top to bottom), the escape time (marked by arrows) increases and fewer ligands escape. The center curve is the fit for the geminate phase of MbCO in water at 25 °C; the dashed line is the single-exponential model (Henry et al., 1983). The nonexponential behavior of the geminate phase is only apparent when it accounts for a substantial fraction of the kinetics.

The middle section of Figure 7 marked "k" shows that when the rate k_{BA} increases by a factor of 10, the geminate phase is shifted to shorter times by a factor of 100, N^{out} decreases, and the escape time is not changed. Data are shown for the β chain of Hb-Zurich–CO in 75% glycerol at 300 K (Dlott et al., 1983), which has the shape characteristic of the diffusion model. The escape time is approximately 30 times smaller than for MbCO.

Section "D" of Figure 7 shows that increasing D shifts the kinetics to slower times by the same factor. Since migration is faster, the escape time decreases and a larger fraction escape.

Figure 8 shows simulations of the diffusion model with data for MbO_2 vs. temperature in 79% glycerol. The data were simulated with $k_{BA} = A \exp[-H/(RT)]$: $H_{BA} = 12$ kJ/mol and $A_{BA} = 5$ cm/s. The channel diffusivity was taken to be the solvent diffusivity/1100 ($D = 5 \times 10^{-9}$ cm^2/s at 300 K) and the equilibrium concentration for the bimolecular phase $c = 1.1 \times 10^5$/cm. The channel growth was taken to be $a = 10$ Å. The choice of channel length directly affects the calculated diffusivity from the observed escape time $\tau_e = a^2/2D$.

Registry No. DDD-heme, 63782-31-0; CO, 630-08-0; CN^-, 57-12-5; O_2, 7782-44-7; CN–protoheme–CN, 37131-16-1; CN–protoheme–CO, 26026-82-4; protoheme, 14875-96-8.

References

Alberding, N., Austin, R. H., Chan, S. S., Einstein, L., Frauenfelder, H., Gunsalus, I. C., & Nordlund, T. M. (1976) *J. Chem. Phys. 65*, 4701–4709.

Antonini, E., & Brunori, M. (1971) *Hemoglobin and Myoglobin in Their Reaction with Ligands*, North-Holland, Amsterdam.

Austin, R. H., Beeson, K. W., Einstein, L., Frauenfelder, H., & Gunsalus, I. C. (1975) *Biochemistry 14*, 5355–5373.

Beece, D. (1983) Ph.D. Thesis, University of Illinois–Urbana.

Beece, D., Eisenstein, L., Frauenfelder, H., Good, D., Marden, M. C., Reinisch, L., Reynolds, A. H., Sorensen, L. B., & Yue, K. T. (1980) *Biochemistry 19*, 5147–5157.

Carslaw, H. S., & Jaeger, J. C. (1959) *Conduction of Heat in Solids*, Oxford University Press, London.

Chernoff, D. A., Hochstrasser, R. M., & Steele, A. W. (1980) *Proc. Natl. Acad. Sci. U.S. A. 77*, 5606–5610.

Collins, F. C., & Kimball, G. E. (1949) *J. Colloid Sci. 4*, 425–437.

Dlott, D. D., Frauenfelder, H., Langer, P., Roder, H., & DiIorio, E. E. (1983) *Proc. Natl. Acad. Sci. U.S.A. 80*, 6239–6243.

Doster, W., Beece, D., Bowne, S. F., DiIorio, E. E., Eisenstein, L., Frauenfelder, H., Reinisch, L., Shyamsunder, E., Winterhalter, K. H., & Yue, K. T. (1982) *Biochemistry 21*, 4831–4839.

Duddell, D. A., Morris, R. J., & Richards, J. T. (1980) *Biochim. Biophys. Acta 621*, 1–8.

Friedman, J. M., Scott, T. W., Fisanick, G. J., Simon, S. R., Findsen, E. W., Ondrias, M. R., & Macdonald, V. W. (1985) *Science (Washington, D.C.) 229*, 187–190.

Gibson, Q. H., & Antonini, E. (1960) *Biochem. J. 77*, 328–341.

Hasinoff, B. B. (1977) *Can. J. Chem. 55*, 3957–3960.

Henry, E. R., Sommer, J. H., Hofrichter, J., & Eaton, W. A. (1983) *J. Mol. Biol. 166*, 443–451.

Jordan, J., Ackerman, E., & Berger, R. L. (1956) *J. Am. Chem. Soc. 78*, 2979–2983.

Keilin, J. (1949) *Biochem. J. 45*, 440–455.

Lindqvist, L., El Mohsni, S., Tfibel, F., Alpert, B., & Andre, J. C. (1981) *Chem. Phys. Lett. 79*, 525–528.

Marden, M. C. (1980) Ph.D. Thesis, University of Illinois–Urbana.

Marden, M. C. (1982) *Eur. J. Biochem. 128*, 399–404.

Martin, J. L., Migus, A., Poyart, C., Lecarpentier, Y., Astier, R., & Antonetti, A. (1983) *Proc. Natl. Acad. Sci. U.S.A. 80*, 173–177.

Noyes, R. M. (1956) *J. Am. Chem. Soc. 78*, 5486-5490.
Noyes, R. M. (1961) *Prog. React. Kinet. 1*, 131-160.
Reynolds, A. H., Rand, S. D., & Rentzepis, P. M. (1981) *Proc. Natl. Acad. Sci. U.S.A. 78*, 2292-2296.
Stetzkowski, F., Banerjee, R., Marden, M. C., Beece, D. K., Bowne, S. F., Doster, W., Eisenstein, L., Frauenfelder, H., Reinisch, L., Shyamsunder, E., & Jung, C. (1985) *J. Biol. Chem. 260*, 8803-8809.

A Raman Spectroscopic Study of Hen Egg Yolk Phosvitin: Structures in Solution and in the Solid State†

B. Prescott,‡ V. Renugopalakrishnan,§ M. J. Glimcher,§ A. Bhushan,‡ and G. J. Thomas, Jr.*,‡

Department of Chemistry, Southeastern Massachusetts University, North Dartmouth, Massachusetts 02747, and Laboratory for the Study of Skeletal Disorders and Rehabilitation, Department of Orthopedic Surgery, Harvard Medical School, Children's Hospital, Boston, Massachusetts 02115

Received November 4, 1985; Revised Manuscript Received January 14, 1986

ABSTRACT: Laser Raman spectroscopy has been employed to study the structure of the hen egg yolk protein phosvitin in H_2O and D_2O solutions at neutral and acidic pH (pD) and in the solid state. The Raman data indicate an unusual conformation for phosvitin in neutral aqueous solution, which is deficient in both α-helix and conventional β-sheet conformations. This unusual pH 7 structure is, however, largely converted to a β-sheet conformation in strongly acidic media (pH <2). β-Sheet is also the predominant secondary structure for phosvitin in the solid state, obtained by lyophilization of the protein from aqueous solution at neutral pH. The imidazolium rings of histidyl residues remain significantly protonated near neutrality, which suggests substantial elevation of the pK for imidazolium ring ionizations of phosvitin in aqueous solution. This may result from extensive ion-pair interactions involving positively charged histidines and negatively charged phosphoserines, which are prevalent in the phosvitin sequence. The present results suggest that antiparallel β-sheets may not be the secondary structure most characteristic of native phosvitin (physiological pH), even though β-sheet is the predominant conformation for phosvitin in acidic solutions (pH 1.5) and in the lyophilized solid. Phosvitin appears to be the first protein for which the major component to the Raman amide I band is centered near 1685 cm^{-1}, which is 10-40 cm^{-1} higher than proteins heretofore examined in aqueous solution by Raman spectroscopy.

Phosvitin, a phosphoglycoprotein of M_r 34 000, is the major protein component of hen egg yolk. The carbohydrate moiety, covalently linked to an asparagine residue, accounts for only about 6.5% of the molecular mass (Shainkin & Perlmann, 1971). The phosvitin sequence of 216 residues is known and exhibits many unusual features, including 123 serines (S),[1] virtually all of which are phosphorylated, 15 lysines (K), 13 histidines (H), and 11 arginines (R) (Byrne et al., 1984). The three-dimensional structure of phosvitin has not yet been determined, and the relevance of the high density of charged side chains to phosvitin function as a transport protein is not known. Accordingly, considerable interest has been focused on the secondary structure of the phosvitin polypeptide chain.

Previous spectroscopic studies suggest several different possibilities for the conformation of the protein chain at physiological pH. Infrared data from D_2O solutions of phosvitin have been interpreted as indicative of an α-helix structure near neutrality (Timasheff et al., 1967). Circular dichroism (CD) investigations, on the other hand, have indicated an irregular structure near neutral pH and a β-sheet structure at acidic pH (Taborsky, 1970; Perlmann & Grizzuti, 1971). NMR results are consistent with an open and flexible structure near pH 7, in which most serine phosphate dianions are accessible to solvent but many of the histidines are not (Vogel, 1983). Recent investigations using CD and Fourier transform infrared (FTIR) spectroscopy have suggested substantial β-sheet conformation in both the solid and solution phases. A secondary structure model has been proposed on the basis of the FTIR spectroscopic results and a secondary structure prediction algorithm (Renugopalakrisnan et al., 1985).

We have undertaken an investigation of the Raman spectrum of phosvitin in the expectation that the Raman data would help to resolve apparent inconsistencies in the previously reported secondary structures. An advantage of Raman spectroscopy is the capability of comparing structural information from both normal and deuterated forms of the protein in solid and solution states. Since interference from liquid water is scant and easily compensated in Raman spectra, the structure-sensitive Raman bands of the protein are easily and reliably compared as a function of the solution pH. The Raman spectrum is also rich in frequencies that originate from vibrations of the amino acid side chains. This property can be exploited to obtain information about the ionization states of phosphoserines and histidines of phosvitin. Interpretation of the conformation-sensitive Raman amide I bands of phosvitin is facilitated by the use of digital methods for both

†Supported by NIH Grants AI11855 (G.J.T.) and AM34078 (M.J.G.) and by the Peabody Home for Crippled Children, Inc.
*Author to whom correspondence should be addressed.
‡Southeastern Massachusetts University.
§Children's Hospital.

[1] Abbreviations: Generally, one-letter symbols are employed for the amino acids. The abbreviation S is used for both serine and phosphoserine. The structure to which it applies is clear from the context in which it is used.

0006-2960/86/0425-2792$01.50/0